



Research article

Anti-enzymatic and DNA docking studies of montelukast: A multifaceted molecular scaffold with *in vitro* investigations, molecular expression analysis and molecular dynamics simulations

Shawana Abdullah^a, Ambar Iqbal^{a,b}, Avinash Karkada Ashok^c, Farah Chafika Kaouche^d, Misbah Aslam^a, Safdar Hussain^a, Jameel Rahman^a, Muhammad Munawar Hayat^e, Muhammad Ashraf^{a,*}

^a Institute of Chemistry, Baghdad-ul-Jadeed Campus, The Islamia University of Bahawalpur, Bahawalpur, 63100, Pakistan

^b Department of Biochemistry and Molecular Biology, Institute of Biochemistry, Biotechnology & Bioinformatics, Baghdad-ul-Jadeed Campus, The Islamia University of Bahawalpur, Bahawalpur, 63100, Pakistan

^c Department of Biotechnology, Siddaganga Institute of Technology, Tumakuru, Karnataka, 572103, India

^d Department of Chemistry, Faculty of Sciences of Mater, Ibn Khaldoun University, BP 78 Zaaoura, 14000, Tiaret, Algeria

^e Punjab Drug Testing Laboratory, P & SH Department, 1-Bird Wood Road, Lahore, Pakistan

ARTICLE INFO

Keywords:

Enzyme inhibition
Molecular expression analysis
MD simulations
Montelukast
DNA docking studies

ABSTRACT

Montelukast, an approved leukotriene receptor 1 (Cys-LT 1) antagonist with anti-inflammatory properties is used for the treatment of asthma and allergic rhinitis. In the present studies, montelukast was subjected to *in vitro* inhibitory assays followed by kinetic and *in silico* investigations. Montelukast demonstrated inhibitory activity against yeast α -glucosidase (IC_{50} 44.31 \pm 1.21 μ M), jack bean urease (JB urease, IC_{50} 8.72 \pm 0.23 μ M), human placental alkaline phosphatase (hPAP, IC_{50} 17.53 \pm 0.19 μ M), bovine intestinal alkaline phosphatase (bIAP, IC_{50} 15.18 \pm 0.23 μ M) and soybean 15-lipoxygenase (15-LOX, IC_{50} 2.41 \pm 0.13 μ M). Kinetic studies against α -glucosidase and urease enzymes revealed its competitive mode of inhibition. Molecular expression analysis of montelukast in breast cancer cell line MCF-7 down-regulated AP by a factor of 0.27 (5 μ M) compared with the 0.26 value for standard inhibitor levamisole (10 μ M). Molecular docking estimated a binding affinity ranging -8.82 to -15.65 kcal/mol for the enzymes. Docking against the DNA dodecamer (ID: 1BNA) observed -9.13 kcal/mol via minor groove binding. MD simulations suggested stable binding between montelukast and the target proteins predicting strong inhibitory potential of the ligand. Montelukast features a chloroquinoline, phenyl ring, a cyclopropane group, a carboxylic group and a sulfur atom all of which collectively enhance its inhibitory potential against the said enzymes. These *in vitro* and computational investigations demonstrate that it is possible and suggested that the interactions of montelukast with more than one targets presented herein may be linked with the side effects presented by this drug and necessitate additional work. The results altogether suggest montelukast as an important structural

* Corresponding author.

E-mail addresses: shawana1abdullah@gmail.com (S. Abdullah), ambar.iqbal@hotmail.com (A. Iqbal), avikarkada@gmail.com (A.K. Ashok), farahchafikakaouche@gmail.com (F.C. Kaouche), asmisbah954@gmail.com (M. Aslam), safdarhussain37@gmail.com (S. Hussain), jameel.rehman@iub.edu.pk (J. Rahman), muhhammadmunawarhayat@yahoo.com (M.M. Hayat), dr.m.ashraf@iub.edu.pk, dr.m.ashraf@gmail.com (M. Ashraf).

<https://doi.org/10.1016/j.heliyon.2024.e24470>

Received 27 September 2023; Received in revised form 6 January 2024; Accepted 9 January 2024

Available online 12 January 2024

2405-8440/© 2024 Published by Elsevier Ltd. This is an open access article under the CC BY-NC-ND license (<http://creativecommons.org/licenses/by-nc-nd/4.0/>).

GIT because of the interactions of mucosal cell lining and bacterial urease, vacuolating cytotoxin (VacA) and cytotoxin-associated gene product (CagA) [16,17]. It is revealed that urease enzyme produces pro-inflammatory immune response by interacting with CD74 cells and causes activation of NF- κ B as well as production of interleukin-8 (IL-8) [18]. These soluble proteins adhere to class II MHC (major histocompatibility complex) present on the gastric epithelial cells and induce their apoptosis, which leads to gastritis and ulcer that can also become gastric cancer [18,19].

Alkaline phosphatases (APs) play fundamental part in the regulation and preservation of phosphate levels in both intracellular and extracellular surroundings. APs hydrolyze phosphodiester bonds from various phosphometabolites and nucleotides and help in cellular absorption of complex molecules. APs are broadly dispersed in all human tissues as four different isozymes, including tissue-specific intestinal (IAP), placental (PAP), and germ cell (GCAP) alkaline phosphatases, and the tissue-nonspecific (TNAP) AP expression in bone, liver, and kidney [20]. The overexpression of these isozymes is linked with many liver diseases, like hepatitis, cirrhosis, bile-duct obstruction, fatty liver, and malignant growths, including breast, colon, prostate, and lung cancers. When AP levels are abnormally elevated in cancer patients, it designates that the sickness has spread to other body parts like the liver, kidney, and bones, inflammation, cardiovascular diseases, vascular calcification and neuronal disorders including Alzheimer's disease (AD) [21].

Most of the diseases are directly or indirectly linked with the commencement of inflammatory processes and if un-treated may involve acute to chronic inflammatory processes. Inflammatory response is initiated when the cellular membranes are damaged due to external or internal insults (Fig. 2). Arachidonic acid and lysophospholipid are released from the damaged phospholipids by the activation of phospholipase A₂. Arachidonic acid is metabolized by cyclooxygenase (COX) pathway at one end and lipoxygenase pathway at another end [22]. The rate limiting enzymes of LOX-pathway are 5-LOX, 12-LOX, 15-LOX which oxidize the corresponding double bonds of the arachidonic acid. The relative hydroperoxyeicosatetraenoic acid (5-HPETE) are formed that further result in the

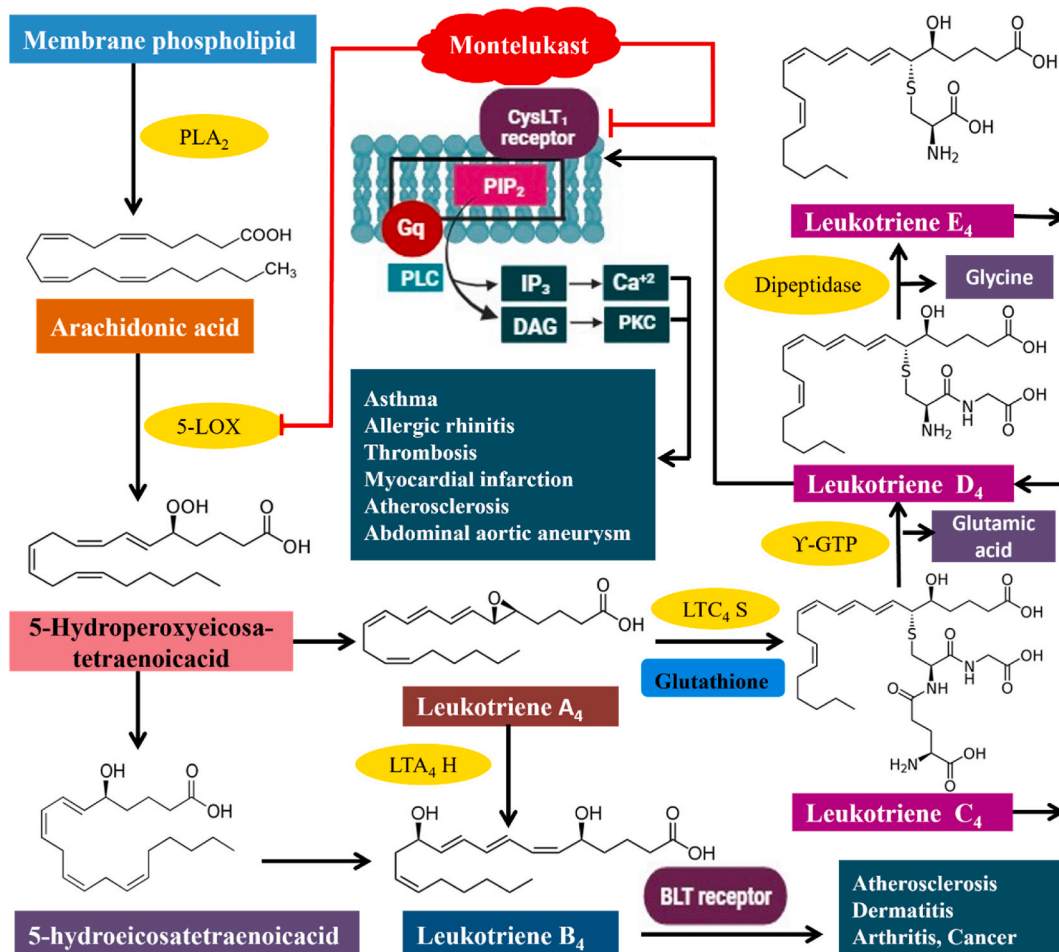


Fig. 2. Arachidonic acid is liberated from membrane phospholipids by the action of phospholipase A₂ (PLA₂) that produces 5-hydroperoxyeicosatetraenoic acid (5-HPETE), LTA₄ and LTB₄ with the help of 5-LOX and lipoxygenase activating protein (FLAP). Subsequently, LTA₄ is converted into LTB₄ and LTC₄ through the actions of LTA₄ H (LTA₄ hydrolase) and LTC₄ S (LTC₄ synthase), respectively. LTC₄ is converted into LTD₄ and LTE₄ via γ -glutamyl transpeptidase (γ GTP) and dipeptidase enzymes, respectively. These three cysteinyl leukotrienes bind Cyst LT1-2 receptors and produce their effects through phospholipase C (PLC) based mechanism. Whereas, LTB₄ may bind BLT1-2 receptors and produce biological effects. Montelukast inhibits 5-LOX, P2Y12 and CysLT₁ receptor which are responsible for triggering various inflammatory responses.

formation of physiologically active mediator molecules, leukotrienes (LTs) [22]. LTA_4 is the first biologically active species which by the enzyme LTA_4 hydrolyze enzyme produces LTB_4 that bind to BLT receptors 1–2 and result in the onset of atherosclerosis, dermatitis, arthritis and some forms of cancer. On the other hand, LTA_4 binds glutathione by the LTC_4 synthase to produce cysteinyl leukotrienes LTC_4 , LTD_4 and LTE_4 which bind Cys-LT receptors 1–2 to produce biological effects including asthma, allergic rhinitis, thrombosis, myocardial infarction, atherosclerosis [1,23]. Montelukast binds the Cys-LT1 receptor, P2Y12 receptor and 5-LOX to relieve the symptoms of these diseases (Fig. 2).

Montelukast structure has many active sites wherein other groups may bind and change its medicinal and pharmacological features. For example, it has a chloroquinoline moiety, phenyl ring, cyclopropane part, carboxylic acid group and a sulfur atom which may contribute towards various pharmacological properties. Keeping in view the above unique structural characteristics of this molecule, this study was aimed to explore its inhibitory activities against α -glucosidase, urease, AP and LOX for the treatment of secondary complications including inflammation, diabetes, ulcer, heart and liver problems and diseases linked to several types of cancers. The present study therefore demonstrates that montelukast effectively but differentially inhibited all the studied enzymes and could serve a promising repurposed molecule beyond its traditional use as a Cys-LT1 receptor antagonist.

2. Experimental

2.1. Materials and methods

The enzymes, substrates and standard inhibitors were purchased from Sigma Aldrich. Montelukast standard (>99.2 % purity) was taken from Punjab Drug Testing Laboratory, Lahore, Pakistan and Multan Drug Testing Laboratory Multan, Pakistan. Rest of the chemicals, methanol, buffers were of analytical/HPLC grade.

2.2. α -Glucosidase inhibition assay

α -Glucosidase inhibition assay was carried out as reported [24]. Briefly, a total volume of 100 μ L contained 70 μ L of 100 mM phosphate buffer pH 6.8, 10 μ L test solution and 10 μ L (0.024 units) of enzyme per well. After mixing and pre-incubating 90 μ L reaction contents, well was pre-read at 405 nm using Synergy HTX BioTek, USA. The reaction was started by the addition of 10 μ L of 0.5 mM substrate solution to a 100 μ L total volume. After 15–20 min, absorbance was read. Both negative and positive (acarbose) controls were included in triplicate assays. The inhibition (%) and IC_{50} value was calculated using EZ-Fit Enzyme Kinetics Software from Perrella Scientific Inc. Amherst, USA. Data was expressed as Mean \pm SEM, $n = 3$. The Inhibition (%) was calculated using the following formula.

$$\text{Inhibition (\%)} = (\text{Abs of control} - \text{Abs of test comp} / \text{Abs of control}) \times 100$$

2.3. Urease inhibition assay

Urease inhibition assay was performed as reported earlier [25]. The reaction mixture contained 50 mM phosphate buffer, 10 μ L test solution and 10 μ L jack bean urease enzyme solution (1 unit/well) per well in a 96-well plate. The contents were mixed, preincubated and 20 μ L of 50 mM urea solution was added to start the reaction. After 15 min incubation, freshly prepared phenol-alkali reagent (60 μ L + 40 μ L) was used to stop the reaction and after color development, the reaction contents were read at 630 nm using 96-well plate reader. The assays were performed in triplicates using both positive (thiourea) and negative controls. Data was expressed as Mean \pm SEM, $n = 3$. The urease activity was expressed by the following formula.

$$\text{Urease inhibition (\%)} = (\text{Abs. of control} - \text{Abs. of test solution} / \text{Abs. of control}) \times 100.$$

Serial dilutions of the test solution were prepared, and their inhibitory profiles were calculated. IC_{50} value was computed as mentioned above.

2.4. Enzyme kinetic studies against α -glucosidase and urease

The kinetic studies were carried out by doing optimized screening assays varying substrate concentrations from zero to 50 μ M and then varying the concentrations of montelukast. For example, it was tested at four concentrations 0, 30, 40 and 44 μ M against α -glucosidase and 0, 1, 16 and 24 μ M against JB urease. The assay data was computed using Prism GraphPad 5.0. The Lineweaver Burk plots were drawn from the data to calculate the kinetic profiles like Michaelis-Menten constant (K_m), maximum velocity (V_{max}) and inhibitory constant (K_i).

2.5. Alkaline phosphatase inhibition assay

The AP assay was carried out by luminescence method with slight modifications as reported [26]. A total volume of 50 μ L assay mixture contained 20 μ L of 3 M DEA buffer, pH 9.8, 10 μ L of test solution and 10 μ L of optimized hPAP or bIAP enzyme solution. After 10 min of pre-incubation at 37 $^{\circ}$ C, the reaction contents were pre-read in luminescence mode of the 96-well plate reader Synergy HTX,

BioTek. Then 10 μL of 250 μM CDP-star® substrate solution was added to initiate the reaction and after 5 min of incubation a change in luminescence signals was measured as post-read value. Levamisole or L-phenylalanine were used as positive controls. Active solutions were serially diluted, and their percentage inhibitions were determined to compute IC_{50} values as mentioned above.

2.6. 15-LOX inhibition assay

The 15-LOX inhibition assay was performed as reported [27]. Briefly, a total volume of 100 μL reaction mixture contained 200 mM borate buffer pH 9.0 (60 μL), test solution (10 μL) and soybean 15-LOX solution (10 μL) and reaction contents (total of 80 μL) were mixed and pre-incubated at 25 °C for 5 min. After given time, 10 μL of 3 nM luminol plus 1 nM cytochrome c solution was added to the reaction mixture per well. Ten μL substrate linoleic acid solution was added to commence the reaction mixture (total of 100 μL). The relative luminescence counts were monitored from 100 to 300 s by 96-well plate Synergy HTX reader in luminescence mode. All experiments were carried out with negative and positive controls in triplicates. The determination of IC_{50} values was carried out as mentioned above for the α -glucosidase enzyme.

2.7. Gene expression analysis in breast cancer cell line MCF-7

The effects of montelukast on the gene expression analysis against tissue nonspecific alkaline phosphatase (TNAP) were demonstrated in the breast cancer cell line MCF-7. Cells were grown in media with standard conditions for 18–24 h with or without the drugs. Cells were harvested, and RNA extracted for further investigations. RNA was extracted with the Trizol method with slight modifications as reported earlier [28]. RNA was quantified by measuring the 260/280 absorbance ratio. cDNA synthesis kit (Vivantis cDSK01-050) was used for synthesis of complementary DNA as per instructions of the manufacturer. Four sets of forward and reverse primers were designed and used. Amplification of cDNA was carried out using Galaxy XP thermal cycler as mentioned earlier using optimized reaction conditions of RT-PCR. The data obtained was analyzed and tabulated (Table 1).

2.8. Computational studies

2.8.1. Structure preprocessing and validation

The Protein Data Bank (PDB) structures of human lysosomal α -glucosidase (ID: 5NN8) crystallized at 2.45 Å resolution [29] through X-ray diffraction method, HP urease (ID: 6ZJA) at 2.00 Å resolution through electron microscopy [30], hPAP (ID: 1ZED) at 1.57 Å resolution through X-ray diffraction method [31], and human 5-LOX (ID: 3V99) at 2.25 Å resolution [32] through X-ray diffraction method were retrieved from Protein Data Bank. Downloaded PDB files were cleaned by removing water molecules and co-crystallized ligands. In order to remodel the incomplete loops, the protein structure from the PDB was used as a template. Proper target-template alignments were made and any missing residues in the structures were homology modeled to generate complete protein models. Subsequently, the generated models were validated through ERRAT [33] and VERIFY3D [34]. The generated models passed the VERIFY3D pass criterion as at least 80 % of the amino acids have scored ≥ 0.1 in the 3D/1D profile. Also, ERRAT quality factor of 90.0887, 96.472, 90.4661 and 92.9771 was observed for 5NN8, 6ZJA, 1ZED and 3V99 models, respectively.

2.8.2. Preparation and molecular docking

The 3D structure of montelukast (PubChem ID: 5281040) was downloaded from the PubChem database (<https://pubchem.ncbi.nlm.nih.gov/>). Active site-based molecular docking with AutoDock4 [35] assisted by AMDock [35] was utilized. The PDB2PQR functionality was utilized to prepare the input files. Search space was defined based on the grid box coordinates around the active site. The grid box dimensions were calculated by expanding the search box until all the active site co-crystallized ligand atoms were covered. For protein human α -glucosidase (ID: 5NN8), grid box coordinates were $X = -14.30$, $Y = -33.80$, $Z = 94.70$ and grid box dimension was set to 28^*28^*28 Å. The important amino acids in the grid box were Asp282, Trp376, Asp404, Leu405, Ile441, Asp443, Trp481, Trp516, Asp518, Met519, Phe525, Arg600, Trp613, Gly 615, Asp616, Asp645, Phe649, Arg672 and His674 (19 amino acids). For HP urease (ID: 6ZJA), the urease subunit beta (chain B) was used with the search space defined around the active site containing nickel atoms in beta subunit. Other chains including Q chain were already removed from the homododecamer during the preparation of the receptor retaining only the active site containing B chain. Grid box coordinates were $X = 223.80$, $Y = 251.40$, $Z = 199.10$ and grid box dimension was set to 39^*48^*43 Å. The key amino acids in the grid box of B-chain were His138, Asn168, Ala169, Kcx219, His221, Glu222, Asp223, His 248, Thr251, Leu252, Ala278, Gly279, Gly280, Gly281, His314, Met317, Leu318, Val320, Cys321, His322, Phe334, Arg338, Ile339, Asp362, Ala365, and Met366 (26 amino acids). The grid box parameters for hPAP (ID: 1ZED) were $X = 38.70$, $Y = 10.10$, $Z = 10.0$ and grid box dimension was set to 62^*48^*70 Å. The important amino acids in the grid box were Asp42,

Table 1
List of primers sequences.

Primers	Temp (°C)	Sequence
ALP_F	58°	ACGAGCTGAACAGGAACAACGT
ALP_R	58°	CACCAGCAAGAAGAAGCCTTTG
GAPDH_F	58°	CGACCACTTTGTCAAGCTC
GAPDH_R	58°	CAAGGGGTCTACATGGCAAC

Asp91, Ser92, Phe107, Gln108, His153, Arg166, Asp316, His317, His320, Glu429, and His432 (13 amino acids). In case of human 5-LOX (ID: 3V99), grid box parameters were X = 19.30, Y = -78.20, Z = -34.10 and grid box dimension was set to 30*30*30 Å. There were 72 amino acids which were found in the grid box from Trp147 to Ala672. Finally, the CHARMM forcefield was utilized with an exhaustiveness of 50 to run 9 docking runs each.

2.8.3. Molecular docking studies against DNA

To investigate the binding interactions between ligand montelukast and DNA, dodecamer DNA (ID: 1BNA) with d (CGCGAATTCGCG)₂ sequence at 1.90 Å resolution [36] through X-ray diffraction method was retrieved in PDB format from the RCSB. After preparation of DNA and ligand, molecular docking was performed in AutoDock 4. The docking results displayed various poses/conformers. The pose with the lowest RMSD and binding affinity was chosen for detailed study. The docked complex was visualized in Discovery Studio. A set of poses was generated, out of which a pose having the least RMSD value with respect to the receptor DNA was selected and value ≤ 2 Å was considered good.

2.8.4. Molecular dynamics simulations, MMPBSA and decomposition analysis

The Molecular Dynamics (MD) simulations of the complexes were conducted using the GROMACS-2020.6 software suite [37]. The initial coordinates were selected based on the optimal docking scored models generated through molecular docking of montelukast with 5NN8, 6ZJA, 1ZED, and 3V99. To set up the simulation, each system was solvated using the TIP3P water model, and they were enclosed within cubic periodic boundary conditions [38]. The dimensions of this box were defined as 100 × 100 × 100, ensuring a minimum of 10 Å of space between the protein and each side of the 3D box, following the approach outlined by Ref. [39]. The parameters for montelukast were generated using the CGenFF tool by CHARMM [40]. Under physiological conditions with a pH of 7.0, the MD simulations were conducted with specific conditions. Periodic boundary conditions were employed to account for the protein residues in their expected ionization states. To neutralize the entire complex, a Monte Carlo ion-placing method was utilized [41]. A force constant of 1000 kJ/mol-nm² was consistently applied throughout all three stages of the MD simulation to restrict the movement of heavy atoms and maintain the native protein folding [42]. The first step involved optimizing the geometry of each system, achieved by performing 50,000 iterations of the steepest descent technique over 50 ps (ps). Subsequently, a two-stage equilibration process was performed, with 250,000 (250 ps) conditioning iterations for each stage. The initial equilibration phase employed a constant NVT ensemble, controlling the number of particles, volume, and temperature. Temperature control was applied using the Berendsen temperature coupling method, as outlined in the method [43]. The second equilibration stage utilized the Parrinello-Rahman barostat within an NPT ensemble set to 1 atm and 303.15 K, following the guidelines [44]. For computing interactions during the 100 ns (ns) of MD simulations, the Particle Mesh Ewald (PME) technique, as described by Darden et al., in 1993 [45], was employed. To ensure stable nanosecond trajectories in highly polar macromolecules like proteins, all covalent bond lengths, including hydrogen bonds, were constrained using the linear constraint LINC technique. The integration time step was set to 2 fs (fs), following Hess et al.'s method from 1997 [46]. The Verlet cut-off approach was used to handle Coulomb, Lennard Jones, and non-bonded interactions within a 10 Å cut-off range, as recommended by Pall and Hess in 2013 [47]. The CHARMM36 m all-atom force field was applied to represent the ions and the protein in the MD simulation. Trajectory analyses were performed by utilizing the built-in capabilities offered by GROMACS.

Using Poisson-Boltzmann surface area (MMPBSA) and molecular mechanics, the binding affinity of the protein-ligand complexes was computed utilizing the GMX_MMPBSA software [48]. Using the Poisson-Boltzmann equation, MMPBSA calculations involved breaking down the total binding affinity into other energetic contributions, such as solvation energy and molecular mechanics (MM) energy as previously explained [49]. While the solvation component uses the Poisson-Boltzmann equation to calculate the system's solvation free energy, considering the electrostatic interactions between the solvent molecules and the solute, the MM component accounts for the molecular mechanics force field terms, such as van der Waals and electrostatic interactions. The decomposition analysis was done by calculating the energy contributions of the amino acid residues in and around 6 Å radius of the active site.

3. Results and discussion

3.1. Enzyme inhibition, kinetic studies and expression analysis

Montelukast was found active against α -glucosidase with IC₅₀ 44.31 ± 1.21 μ M, respectively, compared with the standard acarbose IC₅₀ 370.1 ± 1.11 μ M (Table 2). Lineweaver Burk plot revealed competitive type of inhibition with inhibitory constant (K_i) value of 0.01 μ M (Fig. 3A). This lower K_i value predicts high affinity of montelukast with the enzyme. During the urease inhibitory screening

Table 2

Enzyme inhibition studies of montelukast. Data is Mean ± SEM, n = 3.

IC ₅₀ ±SEM (μ M)				
α -Glucosidase	Urease	hPAP	biAP	15-LOX
44.31 ± 1.21	8.72 ± 0.23	17.53 ± 0.19	15.18 ± 0.23	2.41 ± 0.13

Abbreviations: hPAP (human placental alkaline phosphatase), biAP (bovine intestinal alkaline phosphatase), 15-LOX (15-lipoxygenase). **Standards:** Acarbose against α -glucosidase (IC₅₀ 370.1 ± 1.11 μ M), Thiourea against JB urease (IC₅₀ 21.25 ± 0.15 μ M), L-Phe against bPAP (IC₅₀ 78.42 ± 0.23 μ M), L-Phe against hPAP (IC₅₀ 82.56 ± 0.26 μ M), Baicalein against 15-LOX (IC₅₀ 2.24 ± 0.13 μ M).

assay, montelukast was found as potent inhibitor of urease with IC_{50} value of $8.72 \pm 0.23 \mu\text{M}$ which was very low compared to standard inhibitor thiourea (Table 2). Kinetic analysis depicted that montelukast was a competitive inhibitor of urease enzyme with K_i value of $4.916 \mu\text{M}$, thereby indicating its high affinity with the urease compared to the substrate (Fig. 3B).

Montelukast against the human placental AP (IC_{50} $17.53 \pm 0.19 \mu\text{M}$) and bovine intestinal AP (IC_{50} $15.18 \pm 0.23 \mu\text{M}$) again displayed potent inhibitory profiles as compared with the standards (Table 2). Molecular expression analysis of AP (TNAP) in the breast cancer cell line MCF-7 reported down regulation of this protein at $5 \mu\text{M}$ concentration by 0.27 fold compared with the standard levamisole at $10 \mu\text{M}$ level by 0.26 fold (Table 3). When the montelukast was assayed against the 15-LOX enzyme, the most potent of all enzymes inhibitory profile was revealed with IC_{50} value of $2.41 \pm 0.13 \mu\text{M}$ compared with that of standard baicalein (IC_{50} $2.24 \pm 0.13 \mu\text{M}$).

The inhibitory profiles exhibited by the montelukast display a fascinating structural scaffold with potential to inhibit targeted enzymes of therapeutical importance. These findings have been suggestive of a possible role as anti-inflammatory agent due to 15-LOX inhibition, anticancer agent because of the potent inhibition of AP and down regulation of TNAP in breast cancer cell line [50,51]. *H. pylori* colonizes and causes infection in the stomach lining that in turn ends up in the establishment of inflammation which may be implicated by the montelukast as predicted by *in vitro* screening data against the urease enzyme [52]. The involvement of montelukast in the type 2 DM signaling pathway is also reported in the literature [53]. These are preliminary studies and further investigations are warranted and in no way are of clinical importance until the *in vivo* findings pave the way forward.

3.2. Molecular docking studies

3.2.1. Docking validation

To verify the binding location of the docked ligands, the docked protein-ligand complexes were compared with the respective protein co-crystallized ligand complexes (Fig. 4(A-D)). As observable in Fig. 4(A-D), the docked ligands and the co-crystallized ligands exist in the same active pocket.

3.2.2. Molecular docking studies against human lysosomal α -glucosidase enzyme (ID: 5NN8)

The possible binding mode predictions between montelukast and the human lysosomal α -glucosidase enzyme (PDB ID: 5NN8) were investigated in molecular docking studies, revealing key interactions that stabilize the ligand-receptor complex with a calculated binding affinity of -8.82 kcal/mol (Table 4). The hydroxyl group of the phenyl propanol moiety served as a donor, contributing a hydrogen atom to establish a conventional hydrogen bond with the Phe525. While Arg281 acted as a hydrogen atom donor, forming a conventional hydrogen bond with the oxygen atom of the cyclopropyl acetic acid moiety. Additionally, Ala555 formed alkyl interactions with cyclopropyl group and sulfanyl group of montelukast. Furthermore, Trp516, Trp613 and His674 established π -alkyl interaction with chlorine of chloroquinoline moiety of the ligand. Trp481, Phe649 and Asp616 formed π - π stacked and π -anion interaction with π -electrons of the chloroquinoline ring, respectively. Asp282 also displayed π -anion interactions with the benzyl group of the montelukast. Furthermore, van der Waals interactions involved amino acid residues Leu283, Ala284, Trp376, Asp404, Ile441, Asp518, Asn524, Arg527, Ala554 and Arg600 (Fig. 5(A, A1)). The binding affinity value of -8.82 kcal/mol. These docking studies support the *in vitro* inhibition data of montelukast against the human lysosomal α -glucosidase enzyme.

3.2.3. Molecular docking studies against HP urease (ID: 6ZJA)

The molecular docking studies between montelukast and the HP urease (ID: 6ZJA) receptor elucidated key interactions contributing to the calculated ligand-receptor binding with a binding affinity of -12.38 kcal/mol (Table 4). The phenylpropane and cyclopropyl acetic acid moieties of the ligand established conventional hydrogen bonds by donating their hydrogen atoms to the amino acid

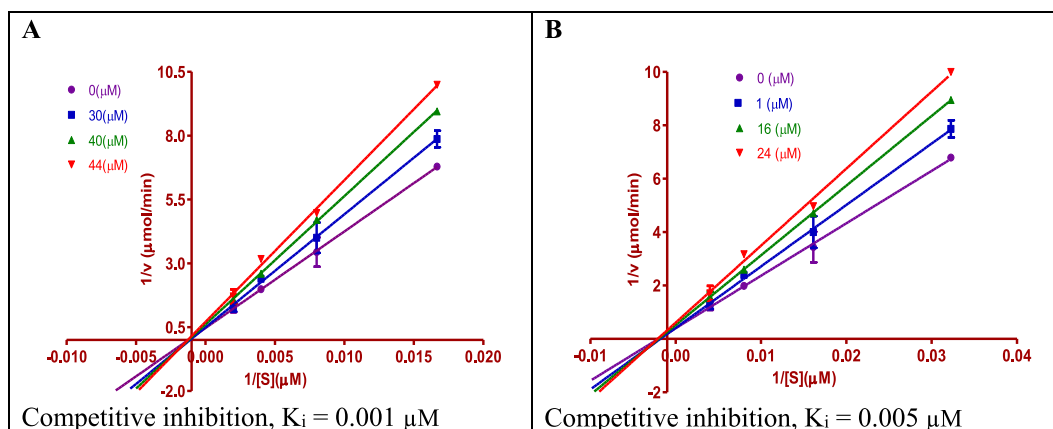


Fig. 3. Demonstration of Lineweaver Burk plot for the calculation of kinetic profiles of montelukast against α -glucosidase (A) and urease enzyme (B).

Table 3

Comparative analysis of montelukast on inhibitory studies of hPAP and bIAP and effects on the regulation of expression of TNAP in breast cancer cell line MCF-7 as compared with standard inhibitor levamisole. The relative expression of control without drugs was considered as 1.0.

PAIs	TNAP Down-regulation
Montelukast (5 μ M)	0.27
Levamisole (10 μ M)	0.26

Note: TNAP (tissue nonspecific alkaline phosphatase).

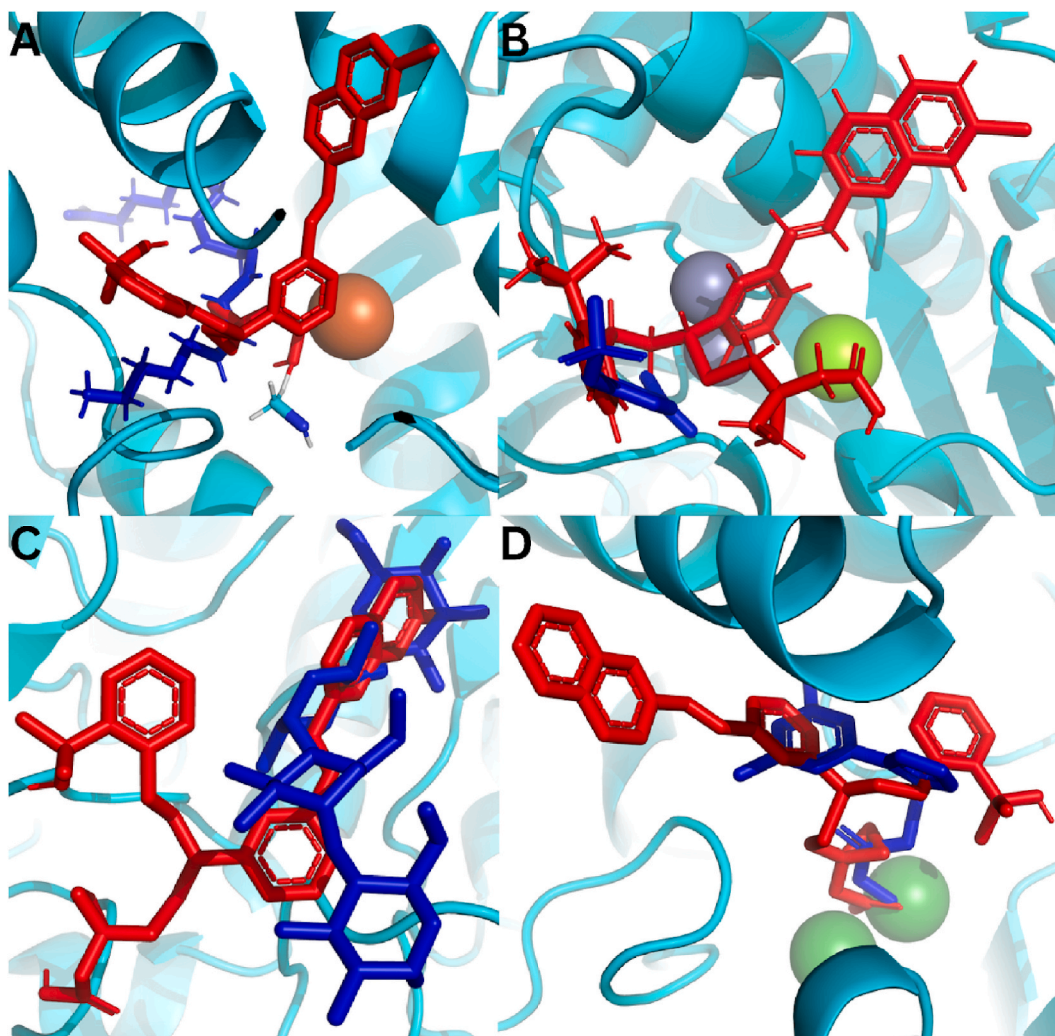


Fig. 4. Montelukast (red) overlapped with the co-crystallized ligand (blue) to validate the docking. (4A) Redocking of montelukast (red) in the active pocket of 5-LOX (PDB ID:3V99) with reference to ligand arachidonic acid (blue). (4B) Redocking of montelukast (red) in the active pocket of AP (PDB ID:1ZED) with reference to co-crystallized ligand *p*-nitrophenyl phosphonate (blue). (4C) Redocking of ligand (red) in the active pocket of α -glucosidase (PDB ID:5NN8) with reference to co-crystallized ligand acarbose (blue). (4D) Redocking of ligand (red) in the active pocket of urease (PDB ID:6ZJA) with reference co-crystallized ligand DJM, i.e., 2- $\{[1-(3,5\text{-dimethylphenyl})\text{-}1\text{H-imidazole-}2\text{-yl]sulfanyl}\}$ -*N*-hydroxyacetamide (blue).

residues Asp223 and Asp362, respectively. Additionally, His248 donated its hydrogen atom to the cyclopropyl acetic acid moiety, forming a carbon-hydrogen bond. Furthermore, Met317 and Cys321 formed carbon-hydrogen bonds with the π -electrons of the chloroquinoline moiety and the phenyl ring of montelukast, respectively. Hydrophobic interactions were observed with His322, Cys321, Ala365, His221, Met371, Val320, and Met366, contributing to the overall stability of the complex. The cyclopropyl acetic acid moiety of the ligand was also involved in a metal interaction. Simultaneously, the phenylpropane ring engaged in a π -lone pair

Table 4

A summary of the docking interactions of proteins and DNA dodecamer with montelukast.

Receptor	*Binding affinity	**LE	Hydrogen bonding	Hydrophobic and other interactions
5NN8 (h-lysosomal α -glucosidase)	-8.82	-0.22	Arg281, Phe525 (conventional hydrogen bond)	Ala555 (alkyl), Trp516, Trp613, His674 (π -Alkyl), Trp481, Phe649 (π - π stacked), Asp282, Asp616 (π -cation), Leu283, Ala284, Trp376, Asp404, Ile441, Asp518, Asn524, Arg527, Ala554, Arg600 (Van der Waals)
6ZJA (HP urease)	-12.38	-0.30	Asp223, Asp362 (conventional hydrogen bond) His248, Met317, Cys321 (C-H bond)	His322 (π - π T-shaped), Cys321, Ala365 (alkyl), His221, His248, Met317, Val320, Met366 (π -alkyl) Ni602 (metal acceptor), His322 (π -lone pair) His136, His138, Ala169, Kcx219, Gly222, Thr251, His274, Gly279, Leu318, Phe334, Arg338 (Van der Waals)
1ZED (hPAP)	-11.87	-0.29	Ser92, Arg166 (conventional hydrogen bond) Val89, His432 (C-H bond)	His88 (π - π stacked), Lys87, Val89, His320, His432, Leu427(π -Alkyl). Zn (metal acceptor), Pro90, Asp91, Phe107, Asp316, His317, Asp428, Glu429, Thr431 (Van der Waals)
3V99 5-LOX	-15.65	-0.38	-	Phe555 (π - π stacked), Leu607(amide- π -stacked), Lys183, Ala606(alkyl), Lys173, Lys183, Tyr660 (π -alkyl). Fe (metal acceptor), Glu172, Gly174, Asp176, Asn180, His367, His372, Ile406, His550, Asn554, Gln557, Tyr558, Asp559, Val604, Ser608, Gln609, Phe610, Arg666, Val671, Ala672 (Van der Waals)
1BNA (DNA dodecamer)	-9.13	-0.22	A: DT7, B: DA18, B: DT20 (Conven-H bond), B: DA18 (C-H bond)	B: DA17 (π -alkyl). A: DA6, A: DT8, A: DC9, A: DG10, B:DG16, B: DT19, B: DC21 (Van der Waals)

*Binding affinity (kcal/mol), **LE = Ligand efficiency (kcal/mol/heavy atoms).

interaction with His322. Furthermore, van der Waals interactions with His136, His138, Ala169, Kcx219, Gly222, Thr251, His274, Gly279, Leu318, Phe334, and Arg338 further strengthened the ligand-receptor binding (Fig. 5(B, B1)). The strong binding affinity supports the *in vitro* inhibition data of montelukast against this HP enzyme (PDB ID: 6ZJA), which may have potential implications for future investigations in urease-related pathologies.

3.2.4. Molecular docking studies against human placental alkaline phosphatase (ID: 1ZED)

The molecular docking studies between montelukast and the human placental alkaline phosphatase (PDB ID: 1ZED) receptor revealed significant interactions that contribute to the ligand-receptor binding with a calculated binding affinity of -11.87 kcal/mol (Table 4). Notably, Ser92 and Arg166 played a crucial role as hydrogen bond donors, forming a conventional hydrogen bond with the oxygen of the cyclopropyl acetic acid moiety. Simultaneously, Val89 and His432 established carbon hydrogen bonds with the π electrons of the phenyl ring and chloroquinoline ring. Additionally, His88 and Lys87 exhibited π - π stacked and π -alkyl interactions with the chloroquinoline group, while Leu427 formed a π -alkyl interaction with the benzene ring of montelukast. Nevertheless, His320 and His432 were engaged in π -alkyl interactions with the cyclopropyl moiety and the adjacent sulfur, respectively. Zn903 demonstrated a metal ion interaction with the acetic acid adjacent to the cyclopropyl group. van der Waals interactions were also demonstrated with amino acid residues Pro90, Asp91, Phe107, Asp316, His317, Asp428, Glu429, and Thr431 (Fig. 5(C, C1)). These findings provide insights into the specific molecular interactions governing the formation of the ligand-receptor complex thus highlighting the support of *in vitro* inhibitory data of montelukast against the said receptor for additional investigations.

3.2.5. Molecular docking studies against 5-LOX (ID: 3V99)

The molecular docking investigations of montelukast with 5-LOX (PDB ID: 3V99) displayed a noteworthy, calculated binding affinity of -15.65 kcal/mol (Table 4). Specifically, within this interaction profile, Lys183 and Ala607 formed alkyl interaction with the methyl of phenyl propanol moiety of montelukast. The amino acids Lys173 and Tyr660 were found to engage in π -alkyl interactions with benzyl and chloroquinoline groups, respectively. The amino acid residues Phe555 and Leu607 played roles in forming π - π stacked and amide- π -stacked interactions with the π electrons of the chloroquinoline and phenyl rings of the ligand, respectively. Furthermore, oxygen of the cyclopropyl acetic acid moiety formed metal interaction with the iron of the protein. Additionally, a network of residues, including Glu172, Gly174, Asp176, Asn180, His367, His372, Ile406, His550, Asn554, Gln557, Tyr558, Asp559, Val604, Ser608, Gln609, Phe610, Arg666, Val671 and Ala672 were involved in van der Waals interactions (Fig. 5(D, D1)). These studies unravel the significance of montelukast as an excellent inhibitor of the LOX enzyme and displaying its features as excellent anti-inflammatory agent.

3.2.6. Molecular docking studies against DNA dodecamer (ID: 1BNA)

The interaction between montelukast with DNA dodecamer [36] was also studied to find any relationship of significance. The minimum energy docked pose of ligand-DNA complexes was selected and are presented (Fig. 6). The results revealed that montelukast interacted with DNA dodecamer via intercalating in minor groove binding with relative binding affinity -9.13 kcal/mol (Table 4).

3.3. MD simulations

3.3.1. Trajectory stability and atomic fluctuations

The four distinct protein structures; human lysosomal- α -glucosidase (ID: 5NN8), HP urease (ID: 6ZJA), hPAP (ID:1ZED), 5-LOX (ID:

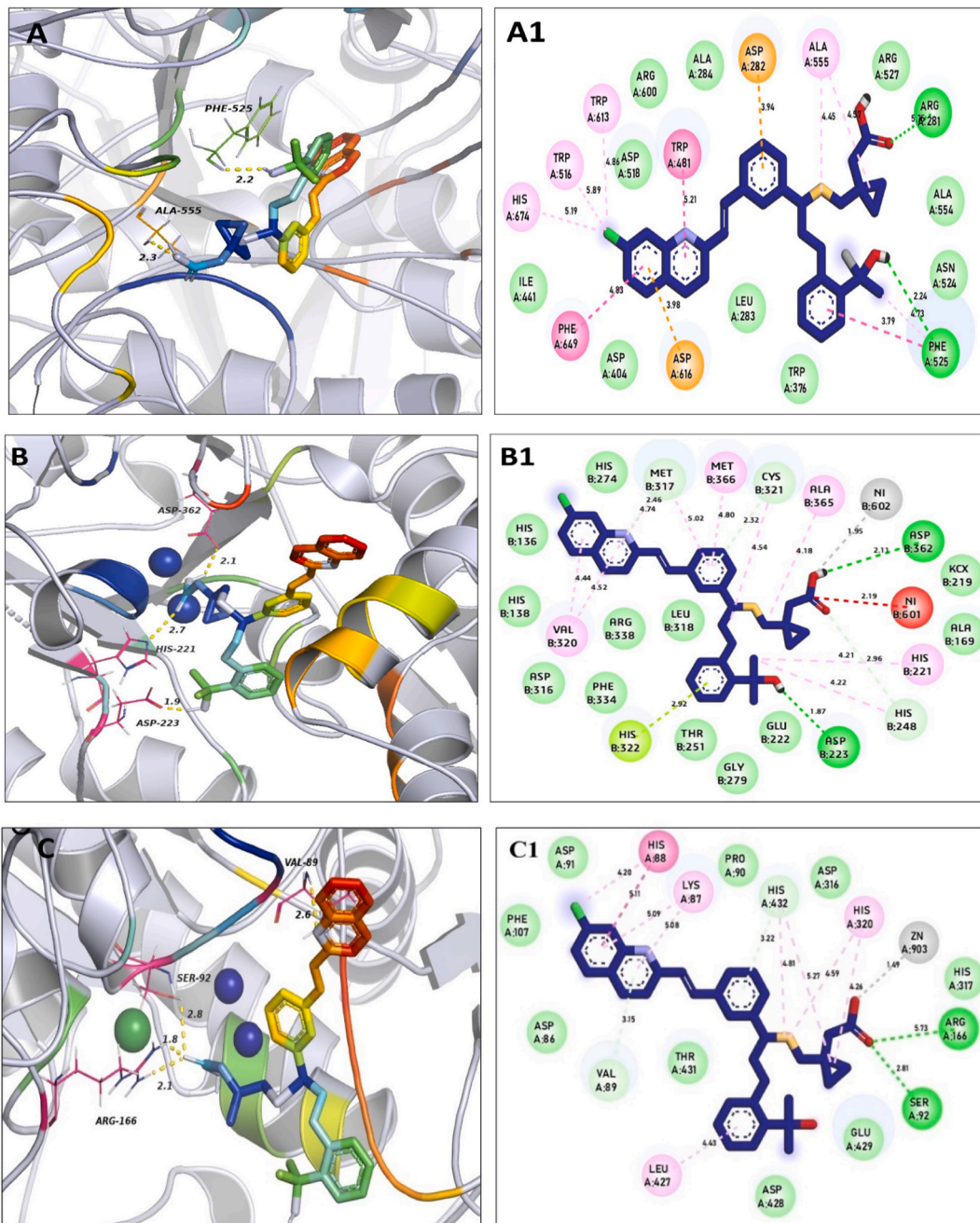


Fig. 5. The 3D (A, B, C, D) and 2D (A1, B1, C1, D1) docking poses of protein ligand complexes using PyMol and Discovery Studio visualizer. The pictures depict binding mode interactions between the proteins human lysosomal α -glucosidase (5NN8, A and A1), HP urease (6ZJA, B and B1), hPAP (1ZED, C and C1), 5-LOX (3V99, D and D1) and the ligand montelukast.

3V99) each forming a complex with the ligand montelukast were classically simulated using GROMACS. All frames of the MD simulation trajectory were meticulously aligned to the initial frame, thereby enabling precise comparisons. The RMSD of the backbone atoms offered insights into the degree of deviation from the input conformation reflecting the dynamic behavior of these complexes during the 100 ns simulation interval. As observable from Fig. 7, the fairly stable trends for the deviations are observed for all the complexes beyond the 20 ns mark indicating stability in the trajectory making it suitable for further analysis. RMSF of the alpha carbon atoms of the amino acid atoms were calculated to assess the flexibility and dynamic behavior of the systems. RMSF quantifies the average deviation of each atom's position from its mean position over the course of the simulation. RMSF calculations can help identify

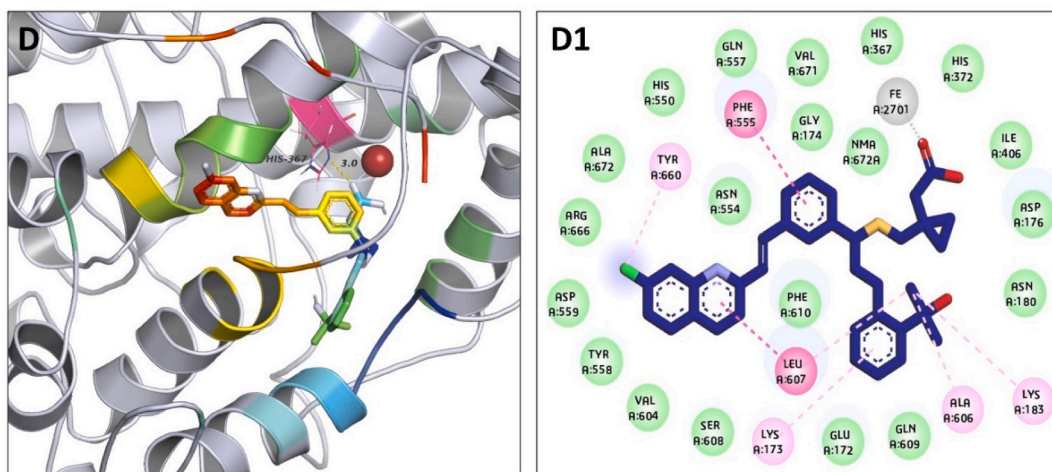


Fig. 5. (continued).

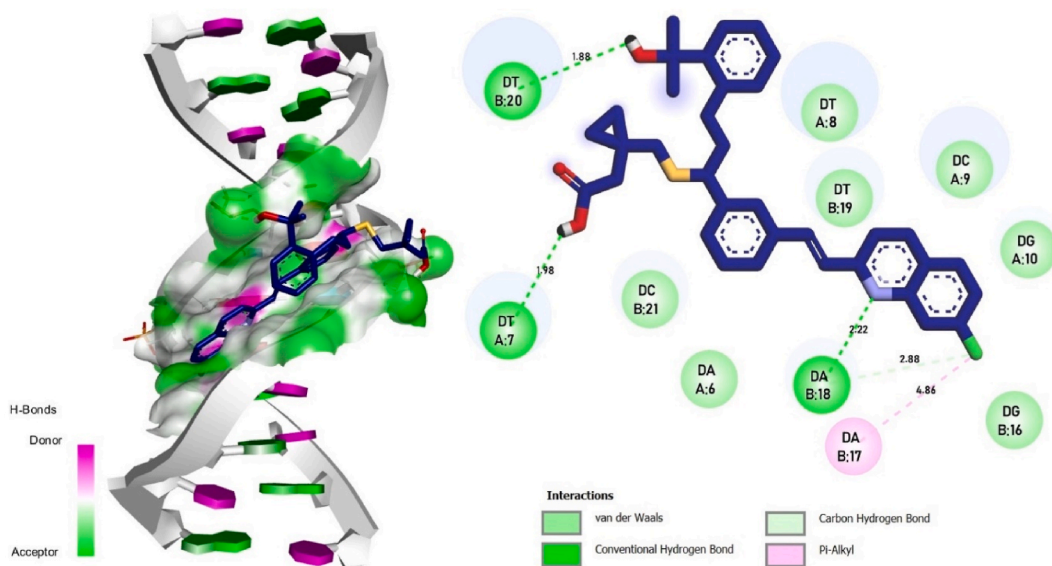


Fig. 6. Binding interactions of montelukast against DNA dodecamer (ID: 1BNA).

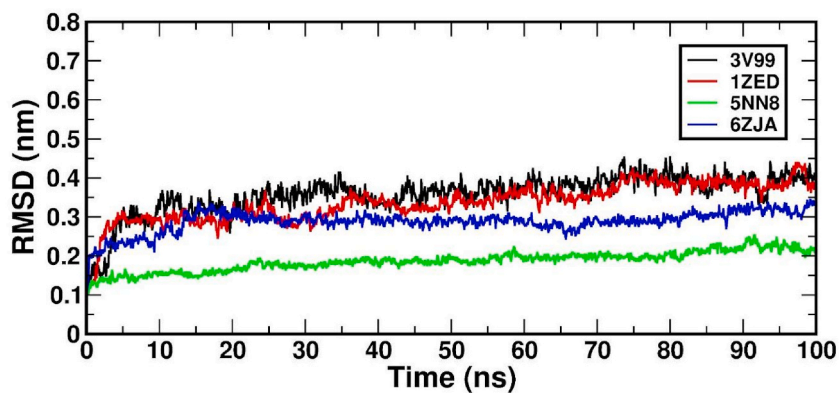


Fig. 7. The RMSD trend plot for the complexes. Frame by frame protein backbone deviations were calculated to generate the deviation plot.

regions that exhibit significant flexibility or rigidity, offering insights into the dynamic behavior of the protein structure. RMSF plots or the systems are indicated in Fig. 8(A-D) with the significant peaks marked. Raw average scores indicate RMSF values of 0.0762 nm, 0.0996 nm, 0.1124 nm and 0.1033 nm for receptors with IDs: 5NN8, 6ZJA, 1ZED and 3V99. Relatively lower fluctuations are observed in the active site residues and the dominant peaks observed in Fig. 8, are projected by looped regions.

3.3.2. Structural compactness and solvent accessible surface area

We monitored the radius of gyration (Rg) and solvent-accessible surface area (SASA) trends, which are the two crucial metrics for characterizing the structural dynamics and interactions of biomolecules. The Rg serves as a fundamental descriptor of a molecular system's overall compactness and conformational variability. Computed as the root mean square distance of atoms from their common center of mass, Rg provides insights into the extent of a molecule's spatial distribution during dynamic simulations. A larger Rg often implies a more extended and flexible structure, while a smaller Rg suggests a more compact and rigid conformation. On the other hand, SASA quantifies the surface area of a biomolecule that is accessible to solvent molecules. It is a valuable indicator of a molecule's exposure to its surrounding environment. During molecular dynamics simulations, SASA helps elucidate how a biomolecular structure interacts with and responds to the solvent. Changes in Rg and SASA trends might indicate structural transitions or instability in the simulated system. Together, Rg and SASA contribute to a comprehensive understanding of the dynamic behavior and structural adaptability of biomolecules under varying environmental conditions in molecular dynamics studies. As observed in Fig. 9(A-C), fairly stable SASA and Rg trends are observed for the systems. This suggests that no significant conformational changes occur that may cause instability in the protein-ligand complex. Upon calculating the average values, it was observed that Rg value of 2.856 nm, 2.465 nm, 2.299 nm and 2.870 nm, and SASA value of 331.553 nm², 243.898 nm², 214.100 nm² and 306.303 nm² was observed for receptors with IDs: 5NN8, 6ZJA, 1ZED and 3V99, respectively.

3.3.3. Molecular mechanics Poisson-Boltzmann surface area (MMPBSA) and decomposition

We adopted the MD based MMPBSA as a computational method to estimate the binding affinity of molecular complexes. This method combines molecular mechanics calculations, Poisson-Boltzmann electrostatics, and solvent-accessible surface area calculations to provide a detailed understanding of the energetics associated with ligand binding to a biomolecular target. The MMPBSA approach involves running extensive molecular dynamics simulations for the protein-ligand complex, the protein alone, and the ligand alone. After obtaining these trajectories, snapshots are extracted at regular intervals. These snapshots are then subjected to energy calculations, where the binding affinity is decomposed into various components, including contributions from van der Waals forces, electrostatic interactions, polar and nonpolar solvation terms, and entropy. Further, residue wise decomposition analysis was done through the breakdown of the overall binding affinity into individual components to identify the key molecular interactions driving the binding affinity. This enabled us to discern the specific residues or regions in the protein that contribute most significantly to the binding, offering valuable insights into the binding energetics. The binding affinity calculated between the receptor and the ligand is indicated in Table 5. As indicated, it is estimated that the montelukast-HP urease receptor complex (ID: 6ZJA-montelukast) has the highest binding affinity of -174 ± 6.23 kcal/mol indicating a significantly strong binding between them. Fig. 10 indicates the residue wise decomposition energy. Prominent energy contributions from Arg166 and Ser92 can be observed in the montelukast-hPAP receptor complex (ID: 1ZED-montelukast). Similarly, contributions from Met366, Ala365, and Cys321 in the HP urease receptor (ID: 6ZJA) complex, Glu172, Tyr181, Ala606, and Glu614 for 3V99, and Arg281, and Arg600 for the α -glucosidase receptor (ID: 5NN8) complex can be observed. Overall, significant binding affinity was estimated between montelukast and the target proteins where relatively higher binding affinity was observed for the HP urease (ID: 6ZJA) and hPAP enzyme (ID: 1ZED).

4. Conclusions

In the present studies montelukast is presented as a multi-targeted, multifaceted molecular scaffold with a potential to bind and inhibit a range of enzymes of therapeutical importance and DNA dodecamer. It inhibited α -glucosidase with IC_{50} 44.31 ± 1.21 μ M in competitive mode supported with *in silico* studies with human lysosomal α -glucosidase. These findings suggest a possible role in reducing the sudden post-prandial rise in blood sugar levels. *In vitro* results have also shown that montelukast inhibited HP urease (IC_{50} 8.72 ± 0.23 μ M), hPAP (IC_{50} 17.53 ± 0.19 μ M), bIAP (IC_{50} 15.18 ± 0.23 μ M) and 15-LOX (IC_{50} 2.41 ± 0.13 μ M). Molecular docking studies predicted a probable binding mode with possible binding interactions with remarkable binding affinity values (-8.82 , -12.38 , -11.87 and -15.65 kcal/mol for α -glucosidase, urease, hPAP and 5-LOX, respectively). Binding interactions with DNA dodecamer displayed -9.13 kcal/mol free energy via intercalation in minor groove binding. Molecular expression analysis in breast cancer MCF-7 cell line down-regulated AP by a factor of 0.27 (5 μ M) compared with the 0.26 (10 μ M) value for standard inhibitor levamisole. MD simulation trajectory analyses indicated stable protein-ligand complexes with no significant conformational changes, thus supporting the *in vitro* profiles. MMPBSA calculations estimated strong binding affinity between montelukast and the protein targets with relatively higher binding affinity values.

Nevertheless, it is already established that montelukast binds the Cys-LT 1 receptor with strong affinity which is implicated in various inflammatory diseases and the progression of cancer. It is ascertained that montelukast contained chloroquinoline, phenyl ring and cyclopropane, carboxylic group as well as sulfur atom that have contributed towards inhibitory potential against the said enzymes too. These *in vitro* and computational investigations demonstrate that the interactions of montelukast with different targets presented herein may be linked with the side effects presented by this drug. There are occasional and indirect reports that montelukast has anti-diabetic, anti-*Helicobacter pylori*, anti-cancer and anti-LOX activities which are complimented with the present investigations and necessitate additional work. The data here presents preliminary findings of montelukast as important molecular structural scaffold

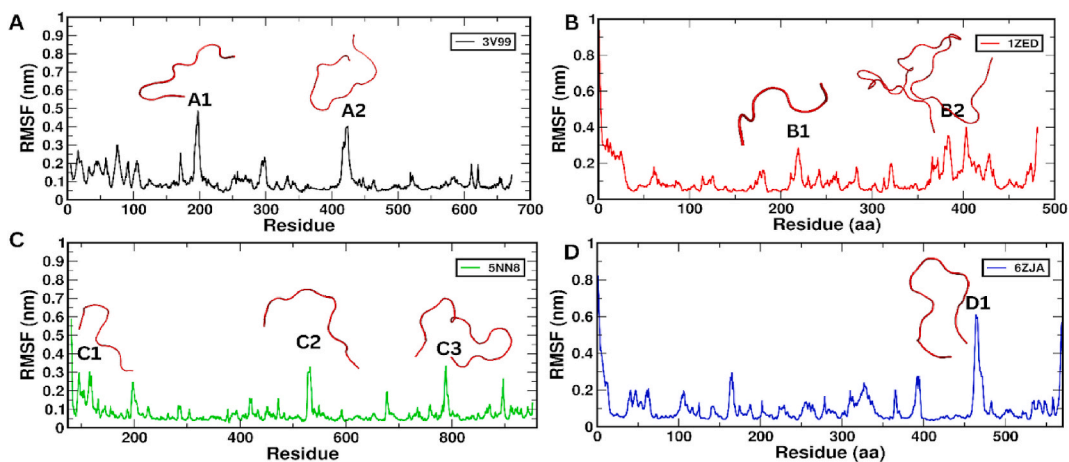


Fig. 8. (A–D). The RMSF profile for the systems. RMSF was calculated based on the $C\alpha$ carbon fluctuation in the MD trajectory. The peaks are marked, and the regions are represented in cartoon models. Looped regions are relatively flexible and generally project higher fluctuations.

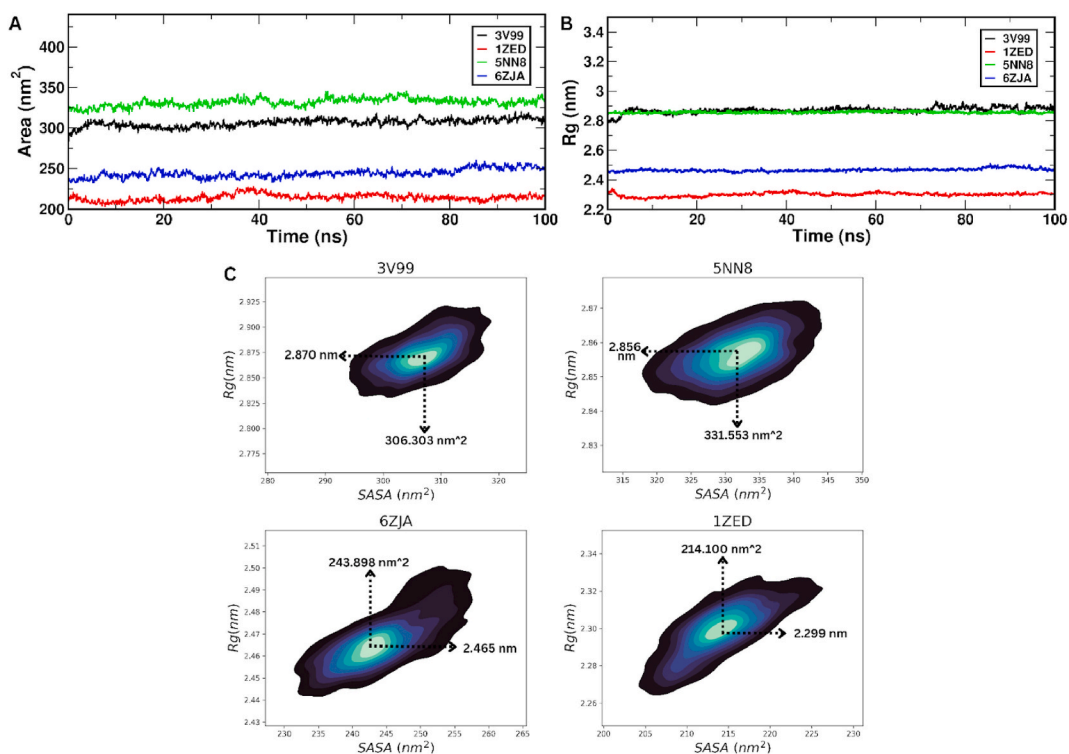


Fig. 9. The SASA trends for the systems are indicated in 9A while the Rg trend is indicated in 9B. 9C is the kernel density estimate plots for the Rg and SASA trajectory data.

Table 5

The summary table of the energy components contributing to the binding affinity.

Energy component	5NN8	6ZJA	1ZED	3V99
ΔG_{GAS} (kcal/mol) = Bond potential term + Angle potential term + Dihedral potential term + Van der Waals contribution + Electrostatic contribution	129.17 ± 3.71	-166.24 ± 2.29	-487.31 ± 3.02	-66.16 ± 2.88
ΔG_{SOLV} (kcal/mol) = Polar and non-polar contribution to the solvation free energy	-130.79 ± 20.83	-8.59 ± 5.80	368.73 ± 0.77	-23.49 ± 0.66
$\Delta TOTAL$ (kcal/mol)	-1.63 ± 21.15	-174.83 ± 6.23	-118.58 ± 3.11	-89.64 ± 2.95

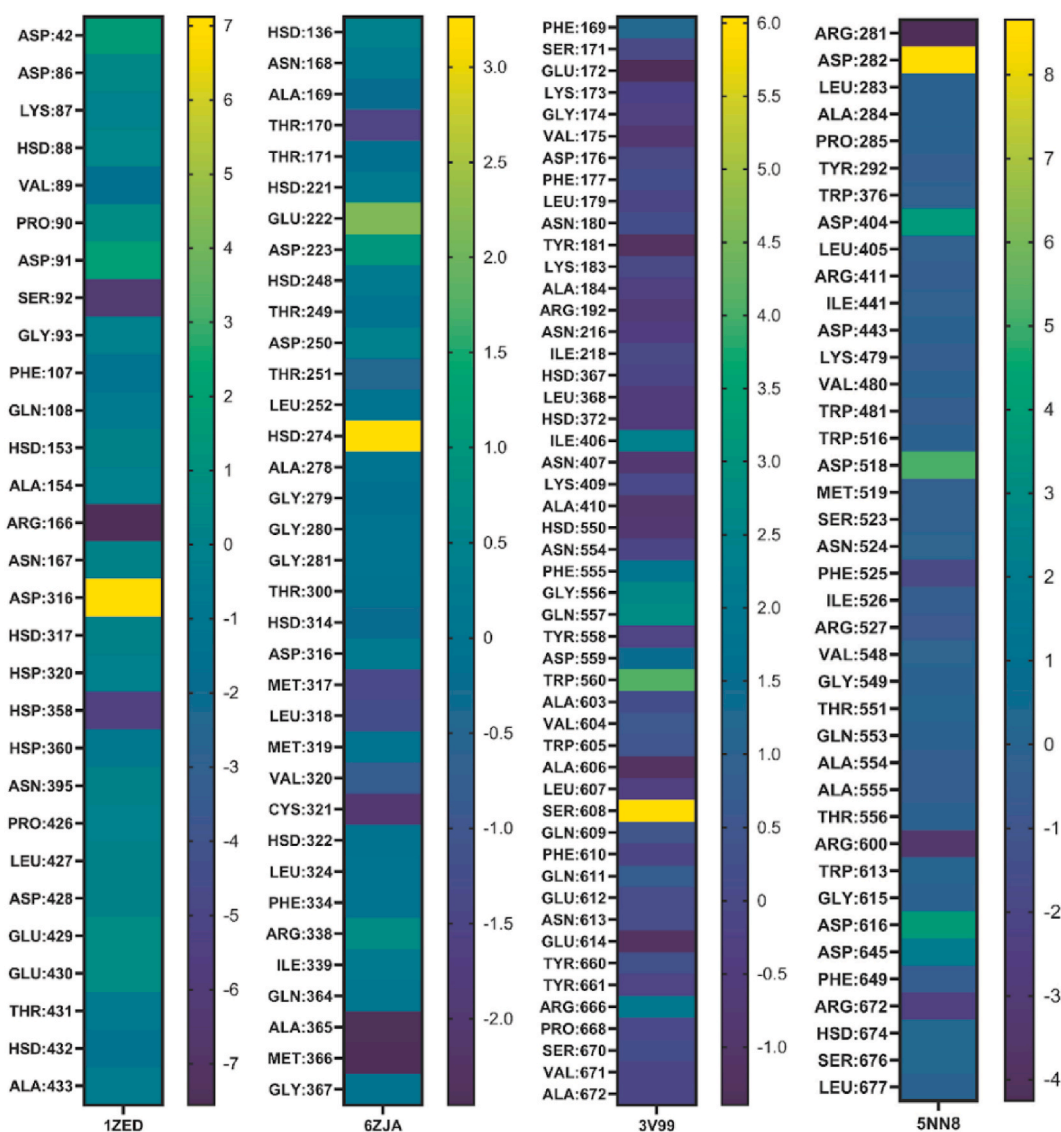


Fig. 10. The residue-wise energy contribution indicated for the complexes in a heat map. The energy values for the residues within 6 Å of the ligand are indicated in kcal/mol.

possessing multitargeted pharmacological features but is inadequate to support the recommendation by a clinician for related disorders until the completion of further investigations to use montelukast as a repurposed drug.

Funding

The presented work was self-funded, and no funding associated with this work was received.

Data availability statement

Whole data is included in this article and is not submitted elsewhere.

Additional information

No additional information is available for this paper.

CRediT authorship contribution statement

Shawana Abdullah: Writing – original draft, Validation, Investigation. **Ambar Iqbal:** Writing – review & editing, Visualization, Validation, Software. **Avinash Karkada Ashok:** Writing – review & editing, Validation, Data curation. **Farah Chafika Kaouche:** Software, Formal analysis. **Misbah Aslam:** Writing – original draft, Methodology, Data curation. **Safdar Hussain:** Validation, Methodology, Data curation. **Jameel Rahman:** Writing – review & editing, Supervision, Formal analysis, Conceptualization. **Muhammad Munawar Hayat:** Resources, Methodology, Formal analysis. **Muhammad Ashraf:** Writing – review & editing, Writing – original draft, Validation, Supervision, Project administration, Formal analysis, Conceptualization.

Declaration of competing interest

The authors declare that they have no known competing financial interests or personal relationships that could have appeared to influence the work reported in this paper.

Acknowledgements

The authors acknowledged the colleagues in the Punjab Drug Testing Laboratory, Lahore (Pakistan) and Multan Drug Testing Laboratory Multan, Pakistan, for the provision of montelukast for the present work.

References

- [1] M. Peters-Golden, W.R. Henderson Jr., Leukotrienes, *New England Journal of Medicine* 357 (18) (2007) 1841–1854, <https://doi.org/10.1056/NEJMra071371>.
- [2] R.C. Gualano, R. Vlahos, G.P. Anderson, What is the contribution of respiratory viruses and lung proteases to airway remodelling in asthma and chronic obstructive pulmonary disease? *Pulm. Pharmacol. Therapeut.* 19 (1) (2006) 18–23, <https://doi.org/10.1016/j.pupt.2005.02.009>.
- [3] A. Theron, C. Gravett, H. Steel, G. Tintinger, C. Feldman, R. Anderson, Leukotrienes C 4 and D 4 sensitize human neutrophils for hyperreactivity to chemoattractants, *Inflamm. Res.* 58 (2009) 263–268, <https://doi.org/10.1007/s00011-008-8049-y>.
- [4] E.D. Bateman, S.S. Hurd, P.J. Barnes, J. Bousquet, J.M. Drazen, M. FitzGerald, P. Gibson, K. Ohta, P. O'Byrne, S.E. Pedersen, Global strategy for asthma management and prevention: GINA executive summary, *Eur. Respir. J.* 31 (1) (2008) 143–178, <https://doi.org/10.1007/s00011-008-8049-y>.
- [5] R. Ramires, M.F. Caiiffa, A. Tursi, J.Z. Haeggström, L. Macchia, Novel inhibitory effect on 5-lipoxygenase activity by the anti-asthma drug montelukast, *Biochemical and biophysical research communications* 324 (2) (2004) 815–821, <https://doi.org/10.1016/j.bbrc.2004.09.125>.
- [6] F. Tahan, E. Jazrawi, T. Moodley, G. Rovati, I. Adcock, Montelukast inhibits tumour necrosis factor- α -mediated interleukin-8 expression through inhibition of nuclear factor- κ B p65-associated histone acetyltransferase activity, *Clin. Exp. Allergy* 38 (5) (2008) 805–811, <https://doi.org/10.1111/j.1365-2222.2008.02963.x>.
- [7] R. Anderson, A.J. Theron, C.M. Gravett, H.C. Steel, G.R. Tintinger, C. Feldman, Montelukast inhibits neutrophil pro-inflammatory activity by a cyclic AMP-dependent mechanism, *Br. J. Pharmacol.* 156 (1) (2009) 105–115, <https://doi.org/10.1111/j.1476-5381.2008.00012.x>.
- [8] G.R. Tintinger, C. Feldman, A.J. Theron, R. Anderson, Montelukast: more than a cysteinyl leukotriene receptor antagonist? *Sci. World J.* 10 (2010) 2403–2413, <https://doi.org/10.1100/tsw.2010.229>.
- [9] M. Hoxha, G.E. Rovati, A.B. Cavanillas, The leukotriene receptor antagonist montelukast and its possible role in the cardiovascular field, *Eur. J. Clin. Pharmacol.* 73 (2017) 799–809, <https://doi.org/10.1007/s00228-017-2242-2>.
- [10] G.O. Dengiz, F. Odabasoglu, Z. Halici, E. Cadirci, H. Suleyman, Gastroprotective and antioxidant effects of montelukast on indomethacin-induced gastric ulcer in rats, *J. Pharmacol. Sci.* 105 (1) (2007) 94–102, <https://doi.org/10.1007/BF02977367>.
- [11] K. Bouchelouche, J. Nordling, T. Hald, P. Bouchelouche, The cysteinyl leukotriene D4 receptor antagonist montelukast for the treatment of interstitial cystitis, *J. Urol.* 166 (5) (2001) 1734–1737, [https://doi.org/10.1016/S0022-5347\(05\)65663-7](https://doi.org/10.1016/S0022-5347(05)65663-7).
- [12] V.B. Nagarajan, P.A. Marathe, Effect of montelukast in experimental model of Parkinson's disease, *Neurosci. Lett.* 682 (2018) 100–105, <https://doi.org/10.1016/j.neulet.2018.05.052>.
- [13] C. Fidan, A. Aydogdu, As a potential treatment of COVID-19: montelukast, *Med. Hypotheses* 142 (2020) 109828, <https://doi.org/10.1016/j.mehy.2020.109828>.
- [14] J.-P.J. Sels, M.S. Huijberts, B.H. Wolffenbuttel, Miglitol, a new α -glucosidase inhibitor, *Expet Opin. Pharmacother.* 1 (1) (1999) 149–156, <https://doi.org/10.1517/14656566.1.1.149>.
- [15] A.S. Dabhi, N.R. Bhatt, M.J. Shah, Voglibose: an alpha glucosidase inhibitor, *J. Clin. Diagn. Res.: J. Clin. Diagn. Res.* 7 (12) (2013) 3023, <https://doi.org/10.7860/JCDR/2013/6373.3838>.
- [16] L.E. Smythies, K.B. Waites, J.R. Lindsey, P.R. Harris, P. Ghiara, P.D. Smith, *Helicobacter pylori*-induced mucosal inflammation is Th1 mediated and exacerbated in IL-4, but not IFN- γ , gene-deficient mice, *J. Immunol.* 165 (2) (2000) 1022–1029, <https://doi.org/10.4049/jimmunol.165.2.1022>.
- [17] A. Covacci, S. Censini, M. Bugnoli, R. Petracca, D. Burroni, G. Macchia, A. Massone, E. Papini, Z. Xiang, N. Figura, Molecular characterization of the 128-kDa immunodominant antigen of *Helicobacter pylori* associated with cytotoxicity and duodenal ulcer, *Proc. Natl. Acad. Sci. USA* 90 (12) (1993) 5791–5795, <https://doi.org/10.1073/pnas.90.12.5791>.
- [18] E.J. Beswick, I.V. Pinchuk, K. Minch, G. Suarez, J.C. Sierra, Y. Yamaoka, V.E. Reyes, The *Helicobacter pylori* urease B subunit binds to CD74 on gastric epithelial cells and induces NF- κ B activation and interleukin-8 production, *Infect. Immun.* 74 (2) (2006) 1148–1155, <https://doi.org/10.1128/iai.74.2.1148-1155.2006>.
- [19] T. Watanabe, M. Tada, H. Nagai, S. Sasaki, M. Nakao, *Helicobacter pylori* infection induces gastric cancer in Mongolian gerbils, *Gastroenterology* 115 (3) (1998) 642–648, [https://doi.org/10.1016/S0016-5085\(98\)70143-X](https://doi.org/10.1016/S0016-5085(98)70143-X).
- [20] R. Lopez-Posadas, R. Gonzalez, I. Ballester, P. Martinez-Moya, I. Romero-Calvo, M.D. Suarez, A. Zarzuelo, O. Martinez-Augustin, F. Sanchez de Medina, Tissue-nonspecific alkaline phosphatase is activated in enterocytes by oxidative stress via changes in glycosylation, *Inflamm. Bowel Dis.* 17 (2) (2011) 543–556, <https://doi.org/10.1002/ibd.21381>.
- [21] M.D. Levitt, S.M. Hapak, D.G. Levitt, Serum ALP–A case report and literature review. Alkaline Phosphatase Pathophysiology with Emphasis on the Seldom-Discussed Role of Defective Elimination in Unexplained Elevations of, *Clinical and Experimental Gastroenterology*, 2022, pp. 41–49, <https://doi.org/10.2147/CEG.S345531>.
- [22] H. Kuhn, S. Banthiya, K. Van Leyen, Mammalian lipoxygenases and their biological relevance, *Biochim. Biophys. Acta Mol. Cell Biol. Lipids* 1851 (4) (2015) 308–330, <https://doi.org/10.1016/j.bbalip.2014.10.002>.
- [23] I. Ivanov, H. Kuhn, D. Heydeck, Structural and functional biology of arachidonic acid 15-lipoxygenase-1 (ALOX15), *Gene* 573 (1) (2015) 1–32, <https://doi.org/10.1016/j.gene.2015.07.073>.
- [24] S. Khan, M. Tariq, M. Ashraf, S. Abdullah, M. Al-Rashida, M. Khalid, P. Taslimi, M. Fatima, R. Zafar, Z. Shafiq, Probing 2-acetylbenzofuran hydrazones and their metal complexes as α -glucosidase inhibitors, *Bioorg. Chem.* 102 (2020) 104082, <https://doi.org/10.1016/j.bioorg.2020.104082>.
- [25] M.U. Khan, M. Aslam, S.A. Shahzad, Z.A. Khan, N.A. Khan, M. Ali, S. Naz, J. Rahman, U. Farooq, Design and synthesis of thiobarbituric acid analogues as potent urease inhibitors, *J. Mol. Struct.* 1231 (2021) 129959, <https://doi.org/10.1016/j.molstruc.2021.129959>.

- [26] E.A. Sergienko, J.L. Millán, High-throughput screening of tissue-nonspecific alkaline phosphatase for identification of effectors with diverse modes of action, *Nat. Protoc.* 5 (8) (2010) 1431–1439, <https://doi.org/10.1038/nprot.2010.86>.
- [27] W. Shahid, S.A. Ejaz, M. Al-Rashida, M. Saleem, M. Ahmed, J. Rahman, N. Riaz, M. Ashraf, Identification of NSAIDs as lipoxigenase inhibitors through highly sensitive chemiluminescence method, expression analysis in mononuclear cells and computational studies, *Bioorg. Chem.* 110 (2021) 104818, <https://doi.org/10.1016/j.bioorg.2021.104818>.
- [28] D.C. Rio, M. Ares, G.J. Hannon, T.W. Nilsen, Purification of RNA using TRIzol (TRI reagent), *Cold Spring Harb. Protoc.* 2010 (6) (2010), <https://doi.org/10.1101/pdb.prot5439> pdb. prot5439.
- [29] V. Roig-Zamboni, B. Cobucci-Ponzano, R. Iacono, M.C. Ferrara, S. Germany, Y. Bourne, G. Parenti, M. Moracci, G. Sulzenbacher, Structure of human lysosomal acid α -glucosidase—a guide for the treatment of Pompe disease, *Nat. Commun.* 8 (1) (2017) 1111, <https://doi.org/10.1038/s41467-017-01263-3>.
- [30] E.S. Cunha, X. Chen, M. Sanz-Gaitero, D.J. Mills, H. Luecke, Cryo-EM structure of *Helicobacter pylori* urease with an inhibitor in the active site at 2.0 Å resolution, *Nat. Commun.* 12 (1) (2021) 230, <https://doi.org/10.1038/s41467-020-20485-6>.
- [31] P. Llinas, E.A. Stura, A. Ménez, Z. Kiss, T. Stigbrand, J.L. Millán, M.H. Le Du, Structural studies of human placental alkaline phosphatase in complex with functional ligands, *J. Mol. Biol.* 350 (3) (2005) 441–451, <https://doi.org/10.1016/j.jmb.2005.04.068>.
- [32] N.C. Gilbert, Z. Rui, D.B. Neau, M.T. Waight, S.G. Bartlett, W.E. Boeglin, A.R. Brash, M.E. Newcomer, Conversion of human 5-lipoxygenase to a 15-lipoxygenase by a point mutation to mimic phosphorylation at Serine-663, *Faseb. J.* 26 (8) (2012) 3222, <https://doi.org/10.1096/fj.12-205286>.
- [33] C. Colovos, T.O. Yeates, Verification of protein structures: patterns of nonbonded atomic interactions, *Protein Sci.* 2 (9) (1993) 1511–1519, <https://doi.org/10.1002/pro.5560020916>.
- [34] R. Luthy, J.U. Bowie, D. Eisenberg, Assessment of protein models with three-dimensional profiles, *Nature* 356 (6364) (1992) 83–85, <https://doi.org/10.1038/356083a0>.
- [35] M.S. Valdes-Tresanco, M.E. Valdes-Tresanco, P.A. Valiente, E. Moreno, AMDock: a versatile graphical tool for assisting molecular docking with Autodock Vina and Autodock4, *Biol. Direct* 15 (1) (2020) 1–12, <https://doi.org/10.1186/s13062-020-00267-2>.
- [36] H.R. Drew, R.M. Wing, T. Takano, C. Broka, S. Tanaka, K. Itakura, R.E. Dickerson, Structure of a B-DNA dodecamer: conformation and dynamics, *Proc. Natl. Acad. Sci. USA* 78 (4) (1981) 2179–2183, <https://doi.org/10.1073/pnas.78.4.2179>.
- [37] V.D. Spoel, GROMACS 2020.6 Source code, Zenodo. doi:<https://doi.org/10.5281/zenodo.4576055>.
- [38] P. Mark, L. Nilsson, Structure and dynamics of the TIP3P, SPC, and SPC/E water models at 298 K, *J. Phys. Chem.* 105 (43) (2001) 9954–9960, <https://pubs.acs.org/doi/10.1021/jp003020w>.
- [39] P. Nayana, H. Manjunatha, P. Gollapalli, A.K. Ashok, P. Karal Andrade, V.V. A combined in vitro and molecular dynamics simulation studies unveil the molecular basis of the anticancer potential of piperine targeting AKT1 against prostate cancer, *J. Biomol. Struct. Dyn.* (2023) 1–14, <https://doi.org/10.1080/07391102.2023.2220045>.
- [40] K. Vanommeslaeghe, E. Hatcher, C. Acharya, S. Kundu, S. Zhong, J. Shim, E. Darian, O. Guvench, P. Lopes, I. Vorobyov, CHARMM general force field: a force field for drug-like molecules compatible with the CHARMM all-atom additive biological force fields, *J. Comput. Chem.* 31 (4) (2010) 671–690, <https://doi.org/10.1002/jcc.21367>.
- [41] G.A. Ross, A.S. Rustenburg, P.B. Grinaway, J. Fass, J.D. Chodera, Biomolecular simulations under realistic macroscopic salt conditions, *J. Phys. Chem. B* 122 (21) (2018) 5466–5486, <https://doi.org/10.1021/acs.jpcc.7b11734>.
- [42] M.A. Helal, S. Shouman, A. Abdelwaly, A.O. Elmeirath, M. Essawy, S.M. Sayed, A.H. Saleh, N. El-Badri, Molecular basis of the potential interaction of SARS-CoV-2 spike protein to CD147 in COVID-19 associated-lymphopenia, *J. Biomol. Struct. Dyn.* 40 (3) (2022) 1109–1119, <https://doi.org/10.1080/07391102.2020.1822208>.
- [43] V. Golo, K. Shahtan, Dynamic attractor for the Berendsen thermostat and the slow dynamics of biomacromolecules, *Biofizika* 47 (4) (2002) 611–617.
- [44] S.C. Tuble, J. Anwar, J.D. Gale, An approach to developing a force field for molecular simulation of martensitic phase transitions between phases with subtle differences in energy and structure, *J. Am. Chem. Soc.* 126 (1) (2004) 396–405, <https://doi.org/10.1021/ja0356131>.
- [45] T. Darden, D. York, L. Pedersen, Particle mesh Ewald: an $N \cdot \log(N)$ method for Ewald sums in large systems, *J. Chem. Phys.* 98 (12) (1993) 10089–10092, <https://doi.org/10.1063/1.464397>.
- [46] B. Hess, H. Bekker, H.J. Berendsen, J.G. Fraaije, LINCS: a linear constraint solver for molecular simulations, *J. Comput. Chem.* 18 (12) (1997) 1463–1472, [https://doi.org/10.1002/\(SICI\)1096-987X\(199709\)18:12<1463::AID-JCC4>3.0.CO;2-H](https://doi.org/10.1002/(SICI)1096-987X(199709)18:12<1463::AID-JCC4>3.0.CO;2-H).
- [47] S. Pall, B. Hess, A flexible algorithm for calculating pair interactions on SIMD architectures, *Comput. Phys. Commun.* 184 (12) (2013) 2641–2650, <https://doi.org/10.1016/j.cpc.2013.06.003>.
- [48] M.S. Valdes-Tresanco, M.E. Valdes-Tresanco, P.A. Valiente, E. Moreno, gmx MMPBSA: a new tool to perform end-state free energy calculations with GROMACS, *J. Chem. Theor. Comput.* 17 (10) (2021) 6281–6291, <https://doi.org/10.1021/acs.jctc.1c00645>.
- [49] A.K. Ashok, T.S. Gnanasekaran, H.S. Santosh Kumar, K. Srikanth, N. Prakash, P. Gollapalli, High-throughput screening and molecular dynamics simulations of natural products targeting LuxS/AI-2 system as a novel antibacterial strategy for antibiotic resistance in *Helicobacter pylori*, *J. Biomol. Struct. Dyn.* (2023) 1–16, <https://doi.org/10.1080/07391102.2023.2210674>.
- [50] N.E. El-Ashrawy, E.G. Khedr, N.F. Khedr, S.A. El-Adawy, Suppression of epithelial-mesenchymal transition and SIRT1/AKT signaling pathway in breast cancer by montelukast, *Int. Immunopharm.* 119 (2023) 110148, <https://doi.org/10.1016/j.intimp.2023.110148>.
- [51] E. Alizamani, B. Ghorbanzadeh, R. Naserzadeh, M.T. Mansouri, Montelukast, a cysteinyl leukotriene receptor antagonist, exerts local antinociception in animal model of pain through the L-arginine/nitric oxide/cyclic GMP/KATP channel pathway and PPAR γ receptors, *Int. J. Neurosci.* 131 (10) (2021) 1004–1011, <https://doi.org/10.1080/00207454.2020.1769618>.
- [52] M.A. Behmanesh, A. Rasekhan, M. Dehghandoost, D.A. Dezfili, B. Ghorbanzadeh, The nitric oxide-cyclic GMP-KATP channels pathway contributes to the effects of montelukast against gastric damage induced by ethanol, *Alcohol* (2023), <https://doi.org/10.1016/j.alcohol.2023.05.008>.
- [53] E. El-Khateeb, E.I. El-Berri, E.M. Mosalam, M.Z. Nooh, S. Abdelsattar, A.M. Alghamdi, S. Alrubia, M.S. Abdallah, Evaluating the safety and efficacy of the leukotriene receptor antagonist montelukast as adjuvant therapy in obese patients with type 2 diabetes mellitus: a double-blind, randomized, placebo-controlled trial, *Front. Pharmacol.* 14 (2023) 1153653, <https://doi.org/10.3389/fphar.2023.1153653>.